Contents list available at IJRED website

Int. Journal of Renewable Energy Development (IJRED)

Journal homepage: https://ijred.undip.ac.id

Research Article

Numerical Study of the Effect of Penstock Dimensions on a Micro-hydro System using a Computational Fluid Dynamics Approach

Yoga Satria Putra[a*], Evi Noviani[b], Muhardi[a]

[a] *Geophysics Department, Faculty of Mathematics and Natural Science, Universitas Tanjungpura, Jl. Prof. Hadari Nawawi, Pontianak, West Kalimantan, Indonesia*

[b] *Mathematics Department, Faculty of Mathematics and Natural Science, Universitas Tanjungpura, Jl. Prof. Hadari Nawawi, Pontianak, West Kalimantan, Indonesia*

Abstract. The performance of a micro-hydro system needs always to be improved so that the electrical power produced can be more optimal. This article aims to study numerically the effect of penstock dimensions on the potential of electrical energy in a micro-hydro system using a computational fluid dynamics (CFD) approach. Studying the impact of dimensions on the performance of a hydropower system is still relatively rare. This paper analyzed the effect of dimensions on the micro-hydro system by constructing thirty simulations of water flow in the penstock. Five variations of penstock slope ($\theta = 50°, 60°, 70°, 80°,$ and $90°$) were generated for six penstock diameter variations ($d = 0.05$ m, 0.10 m, 0.15 m, 0.20 m, 0.25 m, and 0.30 m). The simulations were built using the open-source CFD software OpenFOAM which applies the finite volume method to solve the Navier-Stokes equation as a flow model. The velocity profiles of the simulation are validated against the velocity profile of the analytical solution (power-law) for turbulent flow in the penstock. Analysis of energy loss has been carried out to determine the loss in the penstock that is characterized by the loss coefficient C_L. An enormous C_L value may impact the decrease in the electric power potential of a micro-hydro system. The total length of penstock Lp_T induces the variation of the C_L which affects the changes in the electrical power of the micro-hydro system. The shorter Lp_T will increase the electric power potential of a micro-hydro system. The electric power increases linearly by increasing the penstock's diameter value on a high flow velocity of water in the penstock ($\bar{v} = 10$ m/s). The analysis results show that the penstock dimensions can affect the changes in the electric power of the micro-hydro system. In addition, the work presented in this article has shown that the CFD approach could be used as a low-cost initial step in building an actual micro-hydro system.

Keywords: Micro-hydro, computational fluid dynamics, penstock, OpenFOAM, energy loss, loss coefficient

Article history: Received: 30th Oct 2021; Revised: 5th January 2022; Accepted: 27th January 2022; Available online: 25th February 2022
How to cite this article: Putra, Y.S., Noviani, E., and Muhardi, M. (2022) Numerical Study of The Effect of Penstock Dimensions on a Micro-hydro System using a Computational Fluid Dynamics Approach. *International Journal of Renewable Energy Development,* 11(2), 491-499. https://doi.org/10.14710/ijred.2022.42343

1. Introduction

In general, electricity distribution in developing countries is still not evenly distributed, especially for remote villages. The very far location from the power plant and inadequate road access is the causes electricity cannot be channeled to small villages. One solution from the local government regarding this problem is to build a hydropower plant in villages with the potential for rivers and waterfalls. A hydropower system mostly consists of several components, namely dam, penstock, nozzle, turbine, generator, electrical power storage, and stabilizer. Improving the performance of this system must be continuously conducted to illuminate the remote villages' communities. By optimizing the components of the hydropower system, it will have an impact on increasing the performance of the hydropower system. The study of hydropower as an alternative to electric power has been the concern of researchers to date (Simmons and Lubitz, 2021; Quaranta and Revelli, 2017; Behrouzi *et al.,* 2016; Sangal *et al.,* 2013; Paish, 2002). Many studies have been conducted to optimize the performance of a hydropower system, ranging from small-scale hydropower systems (such as pico-hydro, micro-hydro, and mini-hydro) to large-scale hydropower systems with an electrical power capacity of > 5 MW (Olatunji *et al.,* 2018; Marliansyah *et al.*, 2018; Vermaak *et al.,* 2014, Yahya *et al.,* 2014; Blanco *et al.,* 2008).

Scientists have widely studied the optimization of the components of the hydropower system. Several numerical studies were carried out using a computational fluid dynamics (CFD) approach to design and analyze the performance of water turbines (Pribadyo *et al.,* 2021; Tiwari *et al.,* 2020; Aponte et al., 2020; Arispe *et al.,* 2018; Buono *et al.,* 2015; Bai *et al.*, 2012). The CFD approach may be used to optimize one of the hydropower components, namely the turbine. The modifications on the number and dimensions of turbine blades could affect the performance

* Corresponding author: yogasatriaputra@physics.untan.ac.id

Copyright © 2022. The Authors. Published by CBIORE

of a hydro-turbine. Investigations using the CFD approach have also been conducted in literature to analyze the changes in the number and dimensions of the turbine blades. The dimensions of the turbine blades may influence the efficiency of the turbine to produce electrical power (Wardhana *et al.,* 2019; Arrieta *et al.,* 2013). In addition, the water flow of the hydropower system could affect the performance of a hydro-turbine. One of the challenges in hydropower study is building a hydro-turbine that may operate at low head water flow. Dimensional modification of hydropower components has become a hot topic of increasing the efficiency of a hydropower system (Lee and Lee, 2021; Tafrant and Faizal, 2016; Rohmer *et al*., 2016). In the micro-hydro system, a hydro-turbine may rotate when the river flow has a velocity value > 1.5 m/s. The system may be applied to a low flow river by modifying the appropriate component dimensions (Edeoja and Awuniji, 2017; Singhal and Kumar, 2015). A study on penstock optimization in a low head micro-hydro system has also been carried out to see the effect of increasing the electrical power of a micro-hydro system (Alexander and Giddens, 2008). The effect of penstock angle on changes in electrical power has been performed using the CFD approach (Putra et al. 2021). It has been shown that the penstock angle variation of a micro-hydro system may affect changes in electrical power. Using the CFD approach, a study has shown that energy loss could be reduced by shortening the total length of the penstock.

The previous studies indicate that the dimensions of the hydropower components significantly influence changes in the electrical power of a hydropower system. The investigation related to the performance of a hydropower system mainly emphasizes the turbine components, both numerically and experimentally. The dimensional study on the micro-hydro components is still relatively rare. The present study focuses on the effect of penstock dimensions for the micro-hydro components using the CFD approach. Thirty simulations of water flow were built using the open-source CFD software OpenFOAM. The relationship between the penstock's slope, diameter, and length was analyzed for its effect on electrical power. It makes the difference from previous studies. The study using the CFD approach can be used as a low-cost and safe preliminary study before building the actual design.

2. Methodology

In this study, the work is divided into two parts. The first part is to build a 2D numerical water flow simulation in a penstock.

Table 1
Physical parameters for simulating water flow in the penstock.

Initial flow rate Q_0 (m^3/s)	Inlet diameter d_i (m)	Effective head H_b (m)	Slope θ (°)	Penstock diameter D (m)
0.79	0.20	5.0	50, 60, 70, 80, 90	0.30 0.25 0.20 0.15 0.10 0.07 0.05

The simulations were built using open-source software, OpenFOAM version 6.0. The Reynolds-averaged Navier–Stokes (RANS) model of the k-Epsilon type was used to solve the problem of turbulence in the penstock pipe. The flow model in this study applies the Navier-Stokes equation. This equation is then solved using the finite volume numerical method (Ouafa et al., 2020; Versteeg and Malalasekera, 2007). The computational domain is discretized in a grid using the mesh generation utility of OpenFOAM, *blockMesh*. In OpenFOAM, the boundary conditions of the computational domain are set in a file called *blockMeshDict*, which is located in a folder named *system* (OpenCFD, 2020; Herreras and Izarra, 2013). The flow rate calculation in the penstock is performed on a Linux-based operating system, namely Ubuntu 20.04 LTS. The analysis and visualization of the simulation have been done using an open-source application, Paraview 5.1.2.

In the second part, the analysis of the water discharge was performed on the flow simulations in the penstock. The water flow in the penstock is validated by comparing the simulated velocity profile to the velocity profile of the analytical solution, power-law, for turbulent flow in a pipe. The next step is to analyze the energy loss due to the influence of penstock dimension variations. This step aims to find out how much the penstock dimensions affect the increase in electrical power. The relationship between flow rate and dimensional variations of the penstock has also been analyzed. Finally, the electrical power is calculated based on the OpenFOAM simulation results. The calculated electric power has been compared to the variations of penstock's slope, diameter, and length.

2.1 Computational domain

The 2D computational domain for simulating water flow in the penstock is constructed as Figure 1. The observations are focused on the penstock only (the box with the green dotted line in Figure 1). The grid size in the computational domain is set regularly, namely $\Delta x = \Delta y = 0.002$ m. Based on Figure 1, the water flow from the dam enters a holding tank with a height of $H_t = 1.4$ m and a diameter of $D = 1.05$ m. The initial flow rate that enters through the inlet pipe with a diameter $d_i = 0.2$ m is $Q_0 = 0.79$ m^3/s. The effective head and horizontal penstock lengths are fixed, namely $H_b = 5$ m and $Lp_h = 10$ m, respectively. At the same time, the slope penstock length Lp_s depends on the angle of θ.

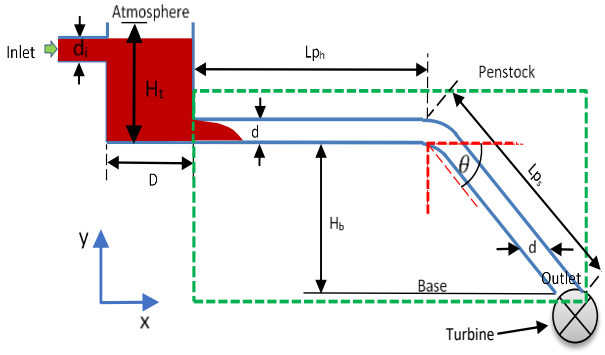

Fig. 1 The geometry of water flow simulation

The five-penstock slope θ are combined with the six-penstock diameter d, as shown in Table 1. The grids in the computational domain are generated using the mesh generation utility of OpenFOAM, namely *blockMesh*. The Dirichlet and Neumann boundary conditions at the inlet, outlet, wall, and atmosphere in the computational domain are organized in a file called *blockMeshDict*, located in the *system*'s folder. The water column in the holding tank is set in the *setFieldsDict* file, which is also located in the *system* folder. This simulation applies the physical properties for water and air, namely the density of water and air, set to ρ_w = 1000 kg/m^3 and ρ_a = 1.1768 kg/m^3, respectively. The viscosity of water and air is set to $\mu_w = 1.85 \times 10^{-5}$ kg/ms and $\mu_a = 1.85 \times 10^{-5}$ kg/ms, respectively, under a gravity acceleration equal to g = 9.81 m/s^2.

2.2 Flow model

The water flow in the penstock is modelled using the Navier-Stokes. This equation was solved using OpenFOAM by applying the finite volume method. The OpenFOAM program code is written in C++ and placed in the OpenFOAM library in a solver. The solver used to solve the flow model is the *interFoam* solver. This solver solves the flow model in the form of continuity and momentum equations which are expressed as:

$$\frac{\partial u_j}{\partial x_j} = 0, \quad (1)$$

$$\frac{\partial u_i}{\partial t} + u_j \frac{\partial u_i}{\partial x_j} = -\frac{1}{\rho}\frac{\partial p}{\partial x_i} + \frac{1}{\rho}\frac{\partial \tau_{ij}}{\partial x_j}, \quad (2)$$

where u, ρ, and p are flow velocity (m/s), fluid density (kg/m^3), and pressure (Pa) respectively. τ_{ij} is stress tensor, which depends linearly on the rate of strain tensor S_{ij} respectively. τ_{ij} and S_{ij} can be defined as:

$$\tau_{ij} = -p\delta_{ij} + 2\mu S_{ij} \text{ and } S_{ij} = \frac{1}{2}\left(\frac{\partial u_i}{\partial x_j} + \frac{\partial u_j}{\partial x_i}\right), \quad (3)$$

where μ is the dynamic viscosity (Ns/m^2). The RANS turbulent model was applied to solve the problem of turbulence in the penstock. The advantage of this model is that the computational effort is relatively low but is entirely accurate for the calculation results. This relatively low computational effort is due to the RANS model solving the Navier-Stokes equation by averaging the velocity against time which is stated in the following equation (Alfonsi, 2009; Gong and Tanner, 2009):

$$\bar{u}(\mathrm{x}) = \frac{1}{T}\int_t^{t+T} u(\mathrm{x}, s)ds, \quad (4)$$

where T is an appropriate time interval (s). Reynolds decomposition of velocity will produce the time-averaged Navier-Stokes equation, which is expressed as the following equation:

$$\frac{\partial \bar{u}_j}{\partial x_j} = 0, \quad (5)$$

$$\frac{\partial \bar{u}_i}{\partial t} + u_j \frac{\partial \bar{u}_i}{\partial x_j} = -\frac{1}{\rho}\frac{\partial \bar{p}}{\partial x_i} + \frac{1}{\rho}\frac{\partial \bar{\tau}_{ij}}{\partial x_j} - \frac{\partial {\tau_{ij}}^R}{\partial x_j}, \quad (6)$$

where ${\tau_{ij}}^R = -\overline{u'_\iota u'_J}$ is the flow fluctuation term. The k-Epsilon model, a semi-empirical model, has been chosen to overcome the turbulence problem in a fluid flow (Harlow and Nakayama, 1968). This model was chosen to solve flow models with a high Reynolds number. The approach taken to obtain the two unknown parameters, k and epsilon, is to solve the following equation:

$$\frac{\partial k}{\partial t} + \bar{u}_i \frac{\partial k}{\partial x_i} = \frac{\partial}{\partial x_j}\left(\nu_{eff}\frac{\partial k}{\partial x_j}\right) + \nu_t \bar{S}^2 - \varepsilon, \quad (7)$$

$$\frac{\partial \varepsilon}{\partial t} + \bar{u}_i \frac{\partial \varepsilon}{\partial x_i} = \frac{\partial}{\partial x_j}\left(\nu_{eff}\frac{\partial \varepsilon}{\partial x_j}\right) + \frac{C_{\varepsilon 1}\nu_t \bar{S}^2 \varepsilon - C_{\varepsilon 2}\varepsilon^2}{k}, \quad (8)$$

where $C_{\varepsilon 1}$ = 1.44, $C_{\varepsilon 2}$ = 1.92, and the mean rate of strain tensor $S = \sqrt{2S_{ij}S_{ij}}$.

2.3 Validation of water flow

The water flow in the penstock from the OpenFOAM simulation needs to be validated to correct the electric power calculation. The velocity profile of the water flow in the simulated penstock is compared with the velocity profile of the analytical solution, power-law, for turbulent flow in a pipe, which is expressed by (Pritchard, 2011):

$$u(r) = u_c\left(1 - \frac{r}{R}\right)^{1/n} \quad (9)$$

where u_c, r, and R are the centerline velocity (m/s), local, and pipe radius (m). The coefficient n is the value associated with the curvature of the velocity profile. The best grid size is determined by testing the water flow simulation in the penstock. Five variations of the regular grid size have been tested by looking at the proximity of the resulting velocity profile pattern to the analytical solution. The regular grid sizes $\Delta x = \Delta y$ used in this test are 0.002 m, 0.004 m, 0.006 m, 0.008 m, and 0.01 m. The relationship between the simulation velocity profile and the analytical solution was analyzed using the Pearson correlation as follows (Young and Freedman, 2007):

$$r = \frac{\sum xy - \frac{(\sum x)(\sum y)}{n}}{\sqrt{\left(\sum x^2 - \frac{(\sum x)^2}{n}\right)\left(\sum y^2 - \frac{(y)^2}{n}\right)}} \quad (10)$$

where r, x, y and n are correlation coefficients, independent variables, dependent variables, and a lot of data, respectively.

The mean squared error (MSE) approach applied to check the estimated error value from the simulation results against the analytical solution, which is expressed in the following equation:

$$MSE = \frac{\sum_{t=1}^{n}(D_{anal} - D_{sim})^2}{n} \quad (11)$$

where D_{anal}, D_{sim},, and n are analytically calculated data, OpenFOAM simulation data, and the amount of data respectively.

2.4 Analysis of electric power

The energy loss of a water flow in the penstock may affect the decrease in the electrical power of a micro-hydro system. This loss could be caused by variations in the total length of the penstock pipe. The energy loss due to the influence of the penstock dimensions can be quantified using the loss coefficients C_L, which are expressed as:

Copyright © 2022. The Authors. Published by CBIORE

$$C_L = \frac{h_L}{\left(\frac{u_{avg}{}^2}{2g}\right)} \quad \text{with } h_L = f\frac{\ell}{D}\frac{u_{avg}{}^2}{2g} \qquad (11)$$

where u_{avg}, h_L, and g are the average velocity (m/s), head loss, acceleration due to gravity (m/s^2). The head loss is defined as a function of the friction factor, total pipe length, pipe diameter, average velocity, and gravity acceleration (Munson et al. 2002). The friction factor f determined using the Moody chart. While the total penstock length is $Lp_T = Lp_h + Lp_s$ where Lp_h is the horizontal penstock length, and Lp_s is the slope penstock length (See Figure 1).

Finally, the electric power P is calculated based on the flow rate in the penstock. The flow rate values need to be known to calculate the electric power. Using the free software Paraview 5.1.2, the flow rate was measured directly at the outlet of the penstock. The electric power P is then calculated easily using the following equation:

$$P = \rho g H_b Q \eta \qquad (12)$$

where ρ, g, H_b, Q, and η are water density (kg/m^3), acceleration of gravity (m/s^2), head height measured from the bottom (m), flow rate (m^3/s), and turbine efficiency (%). In this article, turbine efficiency is not examined directly, so the value of the turbine efficiency is assumed to be 50%.

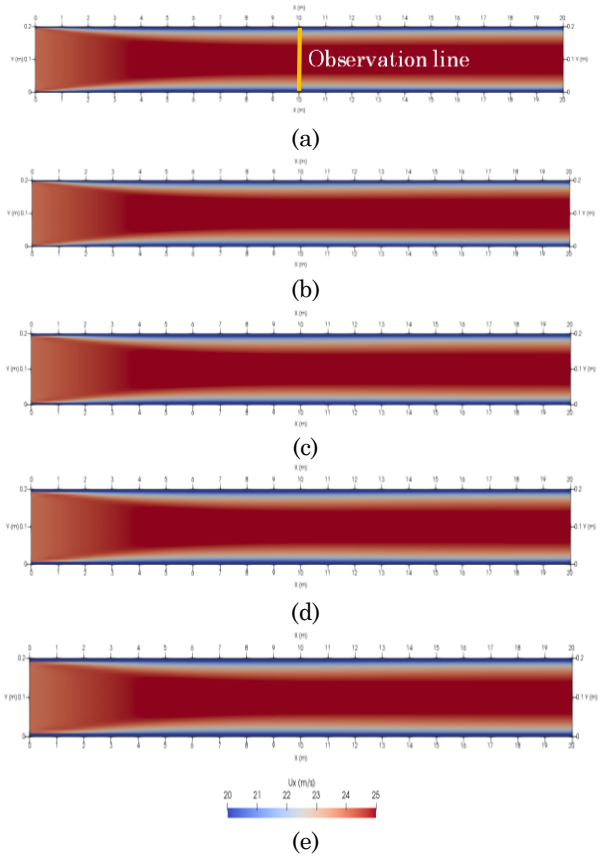

Fig. 2 The velocity fields of water in penstock for five various grid sizes: (a) $\Delta x = \Delta y = 0.002$ m, (b) $\Delta x = \Delta y = 0.004$ m, (c) $\Delta x = \Delta y = 0.006$ m, (d) $\Delta x = \Delta y = 0.008$ m, and (e) $\Delta x = \Delta y = 0.01$ m

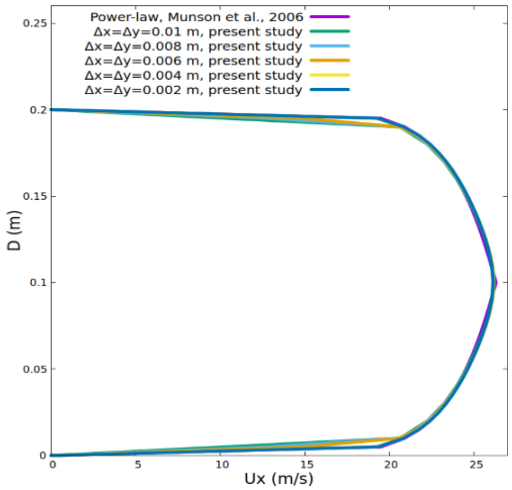

Fig. 3 The simulated water velocity profile compared with the power-law analytical solution (Putra et al. 2021).

3. Validation study

The validation step is essential to produce the correct quantity in the simulation. For this purpose, five simulations of water flow were constructed in a horizontal pipe with length L = 20 m and diameter d = 0.2 m, respectively. The initial flow rate applied to the inlet is Q_0 = 0.79 m^3/s. Water from the inlet is accommodated in a holding tank and then flows into the penstock. The regular grid size of the computational domain has been tested to obtain a good velocity profile, namely $\Delta x = \Delta y$ = 0.002 m, 0.004 m, 0.006 m, 0.008 m, and 0.01 m. The grid test is carried out to determine which grid size may produce a velocity profile closest to the analytical solution's velocity profile.

Figure 2 shows the velocity fields of OpenFOAM simulation results for the water flow in pipes with five variations of grid sizes. Based on these velocity fields can be determined which grid size yields a velocity profile that most closely approximates the analytical solution in equation (9). The velocity profiles have been plotted on the observation line, x = 10 m, for the five velocity fields in Figure 2. The simulated velocity profiles are compared with the calculated velocity profiles using equation (9). The comparison graph of the velocity profile is shown in Figure 3. The figure shows that the simulation has followed the flow principle in a closed channel. The simulated velocity profile has a good agreement with the power-law velocity profile in equation (9).

Table 2
The calculation results of the correlation coefficients R and MSE for the five variations of grid size.

Δx	Δy	R	MSE
0.002	0.002	0.9998	0.0084
0.004	0.004	0.9988	0.0113
0.006	0.006	0.9849	1.0552
0.008	0.008	0.9687	2.3182
0.01	0.01	0.9476	4.1164

Source: Present study (2021)

Copyright © 2022. The Authors. Published by CBIORE

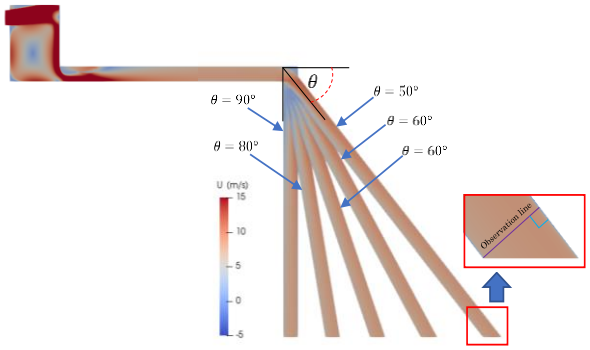

Fig. 4 The simulation results of water flow in a simple micro-hydro system with the diameter $d = 0.30$ m for five variations of the slope $\theta = 50°, 60°, 70°, 80°,$ and $90°$.

At a glance, the velocity profile curve has followed the trend of the analytical solution. The correlation coefficient R and MSE values were calculated on each grid size to determine which value was closest to the reference data. The calculated R and MSE values for the five grid size variations have been summarized as in Table 2. The highest correlation value and the slightest error are $R = 0.9998$ and MSE $= 0.0084$, respectively. These values are obtained from the simulation using a grid size of $\Delta x = \Delta y = 0.002$ m. Based on this test, the grid size $\Delta x = \Delta y = 0.002$ m is the best size to build the water flow simulation in the penstock.

4. Results and Discussion

Thirty simulations of water flow in the penstock have been generated using the CFD approach with the help of open-source software, OpenFOAM. Five simulations were built with different penstock slopes ($\boldsymbol{\theta = 50°, 60°, 70°, 80°}$, and $\mathbf{90°}$) for six different penstock diameters ($d = 0.05$ m, 0.10 m, 0.15 m, 0.20 m, 0.25 m, and 0.30 m). The simulation results on the micro-hydro system are shown in Figure 4. The flow velocity measurement was carried out on the observation line at the penstock outlet using the free software Paraview 5.1.2. The velocity profile is plotted for each variation of the slope and penstock diameter.

4.1 Effect of penstock slope on flow rate

The flow rate in the penstock is one of the physical parameters that determine the value of the electrical power of a micro-hydro system. The effect of penstock slope on flow rate has been analyzed in this step. The calculation of the flow rate was performed to determine this effect. This calculation is done based on the water velocity profile plotted on the observation line. The flow rate profiles at five penstock slopes $\theta = 50°, 60°, 70°, 80°,$ and $90°$ have been plotted for each diameter, namely $d = 0.05$ m, 0.10 m, 0.15 m, 0.20 m, 0.25 m, and 0.30 m as shown in Figure 5. For penstock diameters $d = 0.20$ m, 0.25 m, and 0.30 m (Figure 5(d), (e), and (f)), the flow rate distribution increases as the penstock slope angle (θ) increase from 50° to 90°.

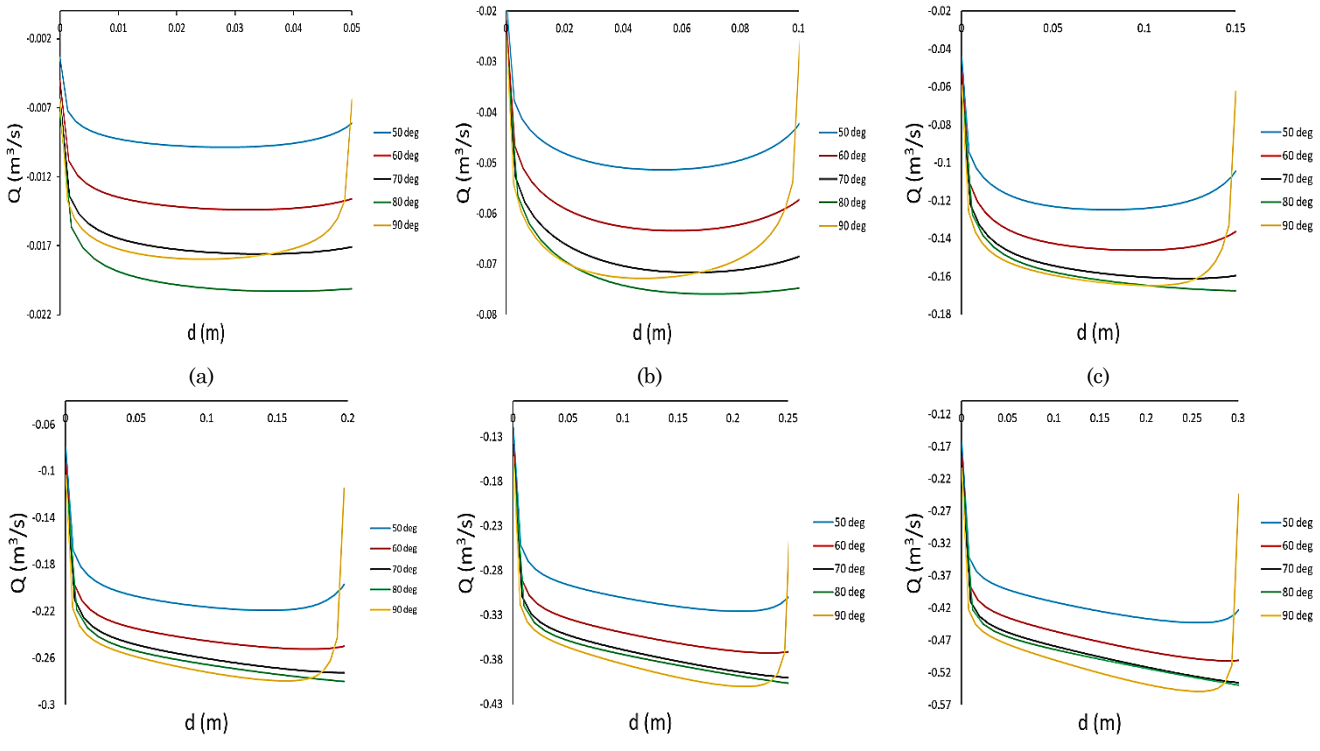

Fig 5. The profile of the water flow rate at the outlet for five variations of the slope ($\theta = 50^o, 60^o, 70^o, 80^o,$ and 90^o) with different diameters: (a) d = 0.05 m, (b) d = 0.10 m, (c) d = 0.15 m, (d) d = 0.20 m, (e) d = 0.25 m, dan (f) d = 0.30 m

Copyright © 2022. The Authors. Published by CBIORE

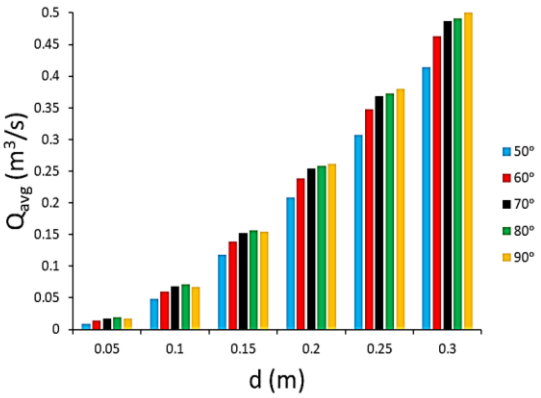

Fig. 6 The average flow rates Q_{avg} on five penstock slopes $\theta = 50°, 60°, 70°, 80°$, and 90° for each diameter $d = 0.05$ m, 0.10 m, 0.15 m, 0.20 m, 0.25 m, and 0.30 m

However, for $d = 0.05$ m, 0.10 m, 0.15 m (Figure 5(a), (b) and (c)), the flow rate decreases on the penstock slope $\theta = 90°$. A high flow velocity ($\bar{v} = 10$ m/s) at a tiny penstock diameter may decrease the flow rate in the penstock with $\theta = 90°$. The elbow penstock's perpendicular angle ($\theta = 90°$) at a too-small diameter will generate the flow reflection effect that reduces the flow rate.

Furthermore, the slope effect was analyzed to see the most significant flow rate in the penstock. For this purpose, the average flow rate Q_{avg} was calculated at the outlet at five penstock slopes. The average flow rate is plotted against the six penstock diameters, as shown in Figure 6. This figure shows that variations in penstock slope may affect the changes in flow rate. The calculations show that the value of Q_{avg} increases with increasing penstock slope for diameters $d = 0.20$ m, 0.25 m, and 0.30 m. The most significant Q_{avg} value occurs at every penstock slope $\theta = 90°$. Meanwhile, the Q_{avg} value decreases at the penstock slope $\theta = 90°$ for $d = 0.05$ m, 0.10 m, and 0.15 m. It indicates that applying a penstock diameter too small for a high-water flow is inappropriate.

4.2 Effect of penstock diameter on flow rate

The diameter effects on the flow rate were analyzed by looking at the flow rate profile for six diameter variations for each slope. The flow rate profiles were plotted against six penstock diameters $d = 0.05$ m, 0.10 m, 0.15 m, 0.20 m, 0.25 m, and 0.30 m for each slope, as shown in Figure 7. This figure shows a pattern of increasing flow rate due to varying penstock diameters. The flow rate may increase for each slope as the diameter of the penstock increases. The profile shows that the outlet's water flow rate seems to be increasing on the inner right side of the penstock. While on the left side of the penstock, the water flow rate has a lower value. The position with the greater flow rate can be considered for designing the nozzle precisely.

The most effective flow rate in the penstock may be observed by looking at the average flow rate Q_{avg}. The Q_{avg} was calculated at six different penstock diameters. The Q_{avg} values for six diameter variations with five penstock slopes have been plotted in Figure 8. This figure shows that the diameter variation affects the change of the Q_{avg} values for five penstock slopes. The lowest average flow rate occurs at the penstock diameter $d = 0.05$ m, while the largest occurs at the penstock diameter $d = 0.30$ m. The flow rate increases linearly with increasing penstock diameter size. The Q_{avg} value is higher at $\theta = 90°$ with $d = 0.30$ m.

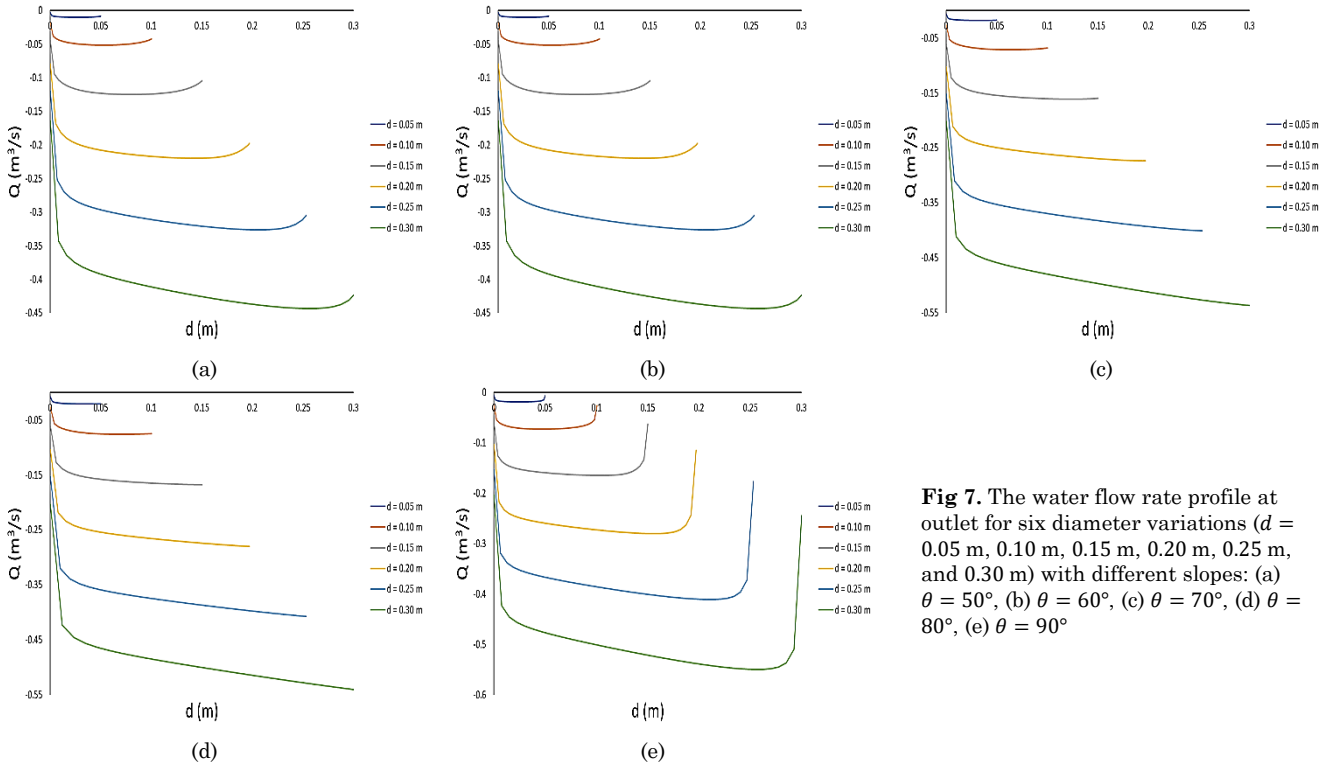

Fig 7. The water flow rate profile at outlet for six diameter variations ($d = 0.05$ m, 0.10 m, 0.15 m, 0.20 m, 0.25 m, and 0.30 m) with different slopes: (a) $\theta = 50°$, (b) $\theta = 60°$, (c) $\theta = 70°$, (d) $\theta = 80°$, (e) $\theta = 90°$

Copyright © 2022. The Authors. Published by CBIORE

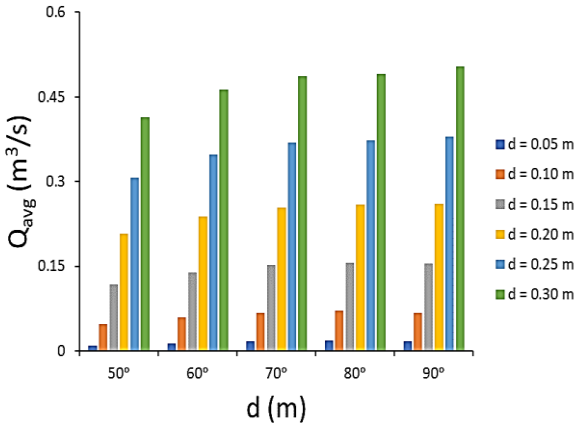

Fig. 8 The average flow rate Q_{avg} at the six diameter variations d = 0.05 m, 0.10 m, 0.15 m, 0.20 m, 0.25 m, and 0.30 m for the five penstock slopes

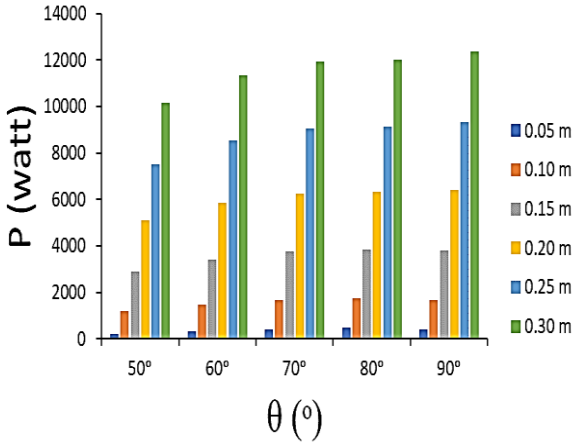

Fig. 10 The effect of penstock slope θ on the electric power potential P at six different diameters d

4.3 Energy loss in the penstock

Based on the previous discussion, the value of Q_{avg} decreases as the penstock slope becomes ramps at $\theta = 50°$. However, when $\theta = 90°$, the value of Q_{avg} becomes larger. The decrease of Q_{avg} is due to the loss of energy from the water flow in the penstock. The energy loss is then analyzed by calculating the loss coefficients C_L using equation (11). The C_L parameter is calculated using the average velocity u_{avg} and the total length of the penstock Lp_T. Both of this information can be measured directly using Paraview from the simulation. The values of C_L were calculated for the five penstock slopes $\theta = 50°$, 60°, 70°, 80°, and 90°. The relationship between the penstock slope and C_L has been plotted as in Figure 9. This figure shows that the ramps penstock slope may increase the C_L value and raise the energy loss in the penstock. The C_L parameter characterizes the energy loss in the penstock. An enormous C_L may reduce the electric power potential of a micro-hydro system. The improvement of C_L is influenced by the total length of the penstock Lp_T. The longest Lp_T may increase the C_L value and reduce the energy in the penstock. These conditions will decrease the electrical power potential of a micro-hydro system.

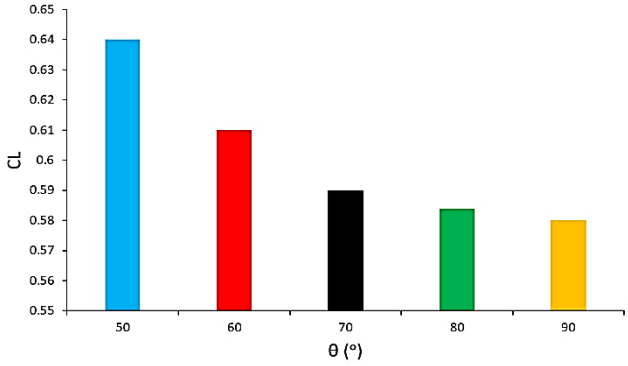

Fig. 9 Relationship between penstock slope θ and loss coefficients C_L

4.4 Effect of penstock dimensions on electric power

The effect of penstock dimensions on electric power P has been analyzed based on the average flow rate Q_{avg}. The electric power potential was calculated for five penstock slopes at each different diameter using equation (12). The relationship between the penstock slope and P at six different diameters was plotted as in Figure 10. This figure shows the increasing electric power due to variations in penstock slope. Increasing electrical power is similar to the average flow rate Q_{avg} due to variations in the penstock slope. It is reasonable because the calculation of the electric power P in equation (12) includes the parameter Q_{avg}, directly proportional to P. The slope of the penstock may affect the electric power P. The $\theta = 90°$ has the smallest total length of penstock Lp_T compared to the other four slopes. The small Lp_T reduce the loss coefficients C_L and improves the micro-hydro system's electric power potential. The significant electric power potential could be achieved for slope $\theta = 90°$ with the high-water velocity in the penstock.

Furthermore, the effect of penstock diameter was analyzed on the electric power potential P of the micro-hydro system. The relationship between penstock diameter concerning P for five different penstock slopes may also be seen in Figure 10. This figure gives the information about increasing electrical power P due to penstock diameter variations. The most significant improvement of P occurred at diameter d = 0.30 m. The combination of large diameter and a penstock slope of $\theta = 90°$ produce the highest electrical power. As discussed previously, the slope of $\theta = 90°$ may decrease the value of loss coefficients C_L, reducing energy losses in the penstock.

4.5 Relationship of penstock length and electric power

The total length of the penstock Lp_T depends on the variations of the penstock slope. The value of Lp_T was measured by using Paraview for each penstock slope. The electrical power P is calculated against five Lp_T for each penstock diameter. The relationship of Lp_T with electrical power for each penstock diameter is shown in Figure 11.

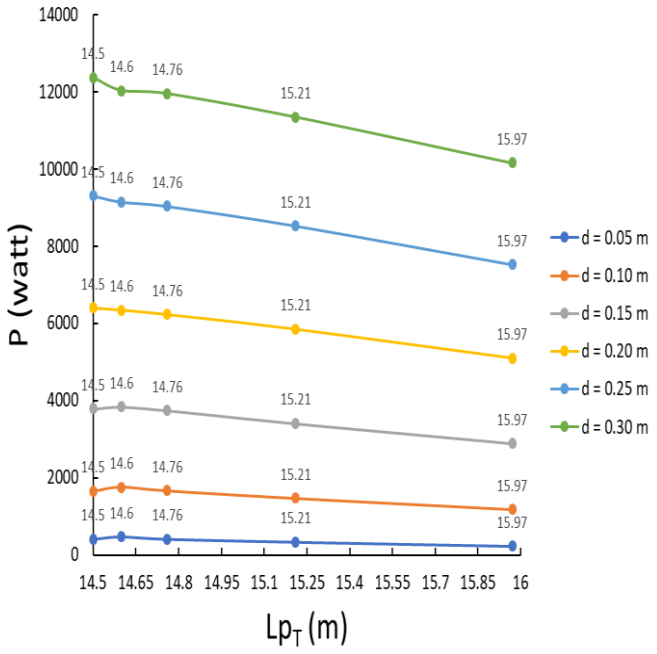

Fig. 11 The relationship of total penstock length Lp_T and electric power P for six penstock diameter variations

The five values of Lp_T in Figure 11 are associated respectively with five penstock slopes, namely $\theta = 50°$, 60°, 70°, 80°, and 90°. Figure 11 shows the decrease of P concerning the Lp_T. For each diameter variation, the significant value of Lp_T causes the decrease of P. Figure 11 shows that a ramps penstock slope ($\theta = 50°$) impact the increase of Lp_T. Meanwhile, improvement of Lp_T may decrease P of a micro-hydro system.

5. Conclusion

Several conclusions have been formulated based on the discussion. Optimizing the components of a hydropower system were performed cheaply and safely using the CFD approach. This work has shown that the CFD approach may be used as an alternative to optimizing the performance of a hydropower system. It can be used as a preliminary study before building a hydropower system in the field. The optimization of hydropower components could be focused on the dimensional analysis of the hydropower system, such as the analysis of the diameter, slope, and length of the penstock carried out in this study. For a micro-hydro system, the increase in electrical power is affected by variations of the penstock's slope, diameter, and length. The electric power P of a micro-hydro system depends on the flow rate distribution in the penstock. The higher flow rate in the penstock increases electric power potential in a micro-hydro system. On the other hand, the reduction of P may be caused by the loss of energy in the penstock. The loss coefficient C_L influences the energy loss in the penstock. An enormous value of C_L will reduce the electric power potential of a micro-hydro system. The longest Lp_T can improve the C_L value and reduce the energy in the penstock. It may impact reducing the electrical power potential of a micro-hydro system. In the future, it is necessary to conduct an experimental study and verify the numerical results in this study.

Acknowledgements

This paper was based on Penelitian Dasar Dipa Untan (PD2U), funded by the DIPA UNTAN grant for the 2021 fiscal year. The computations were done at the Geophysics and GIS Laboratory, Geophysics study program, Faculty of Mathematics and Natural Sciences, Universitas Tanjungpura.

References

Alexander, K.V., Giddens, E.P., (2008)., Optimum penstocks for low head micro hydro schemes. *Renew. Energy,* 33(3), 507-519; doi: 10.1016/j.renene.2007.01.009

Alfonsi, G., (2009). Reynolds-Averaged Navier-Stokes Equations for Turbulence Modelling. *Appl. Mech. Rev*, 62(4); doi: https://doi.org/10.1115/1.3124648

Aponte, R.D., Teran, L.A., Grande, J.F., Coronado, J.J., Ladino, J.A., Larrahondo, F.J., Rodríguez, S.A., (2020). Minimizing erosive wear through a CFD multiobjective optimization methodology for different operating points of a Francis turbine. *Renew Energy,* 145. 2217–2232; doi: 10.1016/j.renene.2019.07.116

Arispe, T.M., de Oliveira, W., Ramirez, R.G., (2018). Francis turbine draft tube parameterization and analysis of performance characteristics using CFD techniques. *Renew Energy,* 127, 114–124; doi: 10.1016/j.renene.2018.04.055

Bai, B., Zhang, L., Guo, T., Liu, C., (2012). Analysis of dynamic characteristics of the main shaft system in a hydro-turbine based on ANSYS. *Procedia Eng*, 31, 654–658; doi: 10.1016/j.proeng.2012.01.1081

Behrouzi, F., Nakisa, M., Maimun, A., Ahmed, Y.M., 2016. Global renewable energy and its potential in Malaysia: A review of Hydrokinetic turbine technology. Renew. Sustain. Energy Rev. 62, 1270-1281. https://doi.org/10.1016/j.rser.2016.05.020.

Blanco, C.J.C., Secretan, Y., Amarante, M.A.L., (2008). Decision support system for micro-hydro power plants in the Amazon region under a sustainable development perspective. *Energy Sust Dev*, 12(3), 25-33.

Buono, D., Frosina, E., Mazzone, A., Cesaro, U., Senatore, A., (2015). Study of a pump as turbine for a hydraulic urban network using a tridimensional CFD modeling methodology. *Energy Procedia,* 82, 201–208; doi: 10.1016/j.egypro.2015.12.020

Edeoja, A.O., Awuniji, L., (2017). Experimental Investigation of the Influence of Penstock Configuration and Angle of Twist of Flat Blades on the Performance of a Simplified Pico-Hydro System. *European Journal of Engineering Research and Science*, 2(7), 14-22; doi: 10.24018/ejers.2017.2.7.401

Gong, Y., Tanner, F.X. (2009). Comparison of RANS and LES models in the laminar limit for a flow over a backward-facing step using OpenFOAM. Nineteenth International Multidimensional Engine Modelling Meeting at the SAE Congress. Detroit, Michigan

Harlow, F.H., Nakayama, P.I., (1968). *Transport of turbulence energy decay rate.* LA-3854, Los Alamos Science Lab. California, USA

Herreras, N., Izarra, J., (2013). Two-Phase pipe flow simulations with OpenFOAM, Master's thesis, Norwegian University of Science and Technology.

Lee, M.D., Lee, P.S., (2021). Modelling the energy extraction from low-velocity stream water by small scale Archimedes screw turbine. *Journal of King Saud University*, In Press, doi: 10.1016/j.jksues.2021.04.006

Marliansyah, R., Putri, D.N., Khootama, A., Hermansyah, H., (2018). Optimization potential analysis of micro-hydro power plant (MHPP) from river with low head. *Energy Procedia*, 153, 74-79. https://doi.org/10.1016/j.egypro.2018.10.021

Munson, B.R., Young, D.F., Okiishi, T.H., (2002). *Fundamentals of fluid mechanics, Fourth Edi*. United States of America: John Wiley & Sons

Copyright © 2022. The Authors. Published by CBIORE

Olatunji, O.A.S., Raphael, A.T., Yomi, I.T, 2013. Hydrokinetic Energy Opportunity for Rural Electrification in Nigeria. Int. Journal of Renewable Energy Development. 7(2), 183-190; doi: http://dx.doi.org/10.14710/ijred.7.2.183-190

OpenCFD. (2020). About OpenFOAM. https://www.openfoam.com/. Accessed on 12 October 2021

Ouafa, M.E., Stéphane, V., Le Chenadec, V., (2020). Navier-Stokes solvers for incompressible single-and two-phase flows. hal-02892344

Paish, O, 2002. Small hydro power: Technology and current status. Renew. Sustain. Energy Rev. 6 (2002), 537–556.

Pribadyo., Hadiyanto., Jamari., (2020). Computational Fluid Dynamic (CFD) Analysis of Propeller Turbine Runner Blades using various Blade Angles. *International Energy Journal,* 21(3), 385-400.

Pritchard, P.J., (2011). *Introduction To Fluid Mechanics*, *Eighth Edi*. United States of America: John Wiley & Sons

Putra, Y.S., Noviani, E., Muhardi., Azwar, A., (2021). Numerical study of the effect of penstock slope on the increase in electric power of micro-hydro system using Computational Fluid Dynamics. *IOP Conference Series: Earth and Environmental Science (EES*). Yogyakarta, Indonesia

Quaranta, E., Revelli, R., (2017). Gravity water wheels as a micro hydropower energy source: a review based on historic data, design methods, efficiencies and modern optimizations. *Renew Sustain Energy Rev*. 97, 414-427.

Rohmer, J., Knittel, D., Sturtzer, G., Flieller, D., Renaud, J., (2016). Modeling and experimental results of an Archimedes screw turbine. *Renewable Energy*, 94, 136-146; doi: 10.1016/j.renene.2016.03.044

Sangal, S., Garg, A., Kumar, D., 2013. Review of optimal selection of turbines for hydroelectric projects. Rev. Optim. Sel. Turbines Hydroelectr. Proj. 3, 424–430.

Simmons, S.C., Lubitz, W.D., 2021. Archimedes screw generators for sustainable micro-hydropower production. *International Journal of Energy Research*, 45(12), 17480-17501; doi: 10.1002/er.6893

Singhal, M.K., Kumar, A., (2015). Optimum Design of Penstock for Hydro Projects. International Journal of Energy and Power Engineering, 4(4), 216-226; doi: 10.11648/j.ijepe.20150404.14

Tafrant, D., Faizal, M., (2016). The effect of fluid flow current to 300 blades Achard turbine performance. *Journal of Mechanical Science and Engineering*, 3(1), 7-12

Tiwari, G., Kumar, J., Prasad, V., Patel, V. K., (2020). Utility of CFD in the design and performance analysis of hydraulic turbines-A review. *Energy Reports,* 6, 2410-2429; doi: 10.1016/j.egyr.2020.09.004

Vermaak, H.J., Kusakana, K., Koko, S.P., (2014). Status of microhydrokinetic river technology in rural applications. Renewable and Sustainable Energy Reviews, 29, 625 – 633; doi: https://doi.org/10.1016/j.rser.2013.08.066

Versteeg, H.K., Malalasekera, W., (2007). *An introduction to computational fluid dynamics: the finite volume method, second edi.* England: Pearson Education Limited

Wardhana, E.M., Santoso, A., Ramdani, A.R., (2019). Analysis of Gottingen 428 airfoil turbine propeller design with computational fluid dynamics method on gravitational water vortex power plant. *Int. J. Mar. Eng. Innov. Res,* 3(3); doi: 10.12962/j25481479.v3i3.4864

Yahya, A.K., Munim, W.N.W.A., Othman, Z., (2014). Pico-hydro power generation using dual pelton turbines and single generator. *IEEE 8th International Power Engineering and Optimization Conference (PEOCO2014)*, 579-584; doi: 10.1109/PEOCO.2014.6814495.

Young, H.D., Freedman, R.A. (2007). *University physics 12th edition.* Pearson-Addison Wesley, New York

© 2022. The Authors. This article is an open access article distributed under the terms and conditions of the Creative Commons Attribution-ShareAlike 4.0 (CC BY-SA) International License (http://creativecommons.org/licenses/by-sa/4.0/)